Original Article

JCBFM

Journal of Cerebral Blood Flow & Metabolism
2018, Vol. 38(10) 1796–1806

DOI: 10.1177/0271678X17718436
journals.sagepub.com/home/jcbfm
SAGE

Metabolic regional and network changes in Alzheimer's disease subtypes

Karl Herholz[1,2], Cathleen Haense[1], Alex Gerhard[1,2,3,4], Matthew Jones[2,3], José Anton-Rodriguez[1], Shailendra Segobin[1], Julie S Snowden[2,3], Jennifer C Thompson[2,3] and Christopher Kobylecki[2,3]

Abstract

Clinical variants of Alzheimer's disease (AD) include the common amnestic subtype as well as subtypes characterised by leading visual processing impairments or by multimodal neurocognitive deficits. We investigated regional metabolic patterns and networks between AD subtypes. The study comprised 9 age-matched controls and 25 patients with mild to moderate AD. Methods included clinical and neuropsychological assessment, high-resolution FDG PET and T1-weighted 3D MR imaging with PET-MR coregistration, grey matter segmentation, atlas-based regions-of-interest, linear mixed effects and regional correlation analysis. Regional metabolic patterns differed significantly between groups, but significant hypometabolism in the posterior cingulate cortex (PCC) was common to all subtypes. The most distinctive regional abnormality was occipital hypometabolism in the visual subtype. In controls, two large clusters of positive regional metabolic correlations were observed. The most pronounced breakdown of the normal correlation pattern was found in amnestic patients who, in contrast, showed the least regional focal metabolic deficits. The normal positive correlation between PCC and hippocampus was lost in all subtypes. In conclusion, PCC hypometabolism and metabolic correlation breakdown between PCC and hippocampus are the common functional core of all AD subtypes. Network alterations exceed focal regional impairment and are most prominent in the amnestic subtype.

Keywords

Alzheimer's disease, brain imaging, dementia, energy metabolism, positron emission tomography

Received 27 February 2017; Revised 10 May 2017; Accepted 19 May 2017

Introduction

Alzheimer's disease (AD) is commonly characterized by a leading impairment of episodic memory, which is associated with dysfunction and atrophy of allocortical structures located in the mesial temporal lobe, such as the hippocampus.[1] However, there are also focal subtypes of AD with leading impairment of cognitive functions other than episodic memory.[2] These include posterior cortical atrophy with leading impairment of visual functions and logopenic aphasia with leading impairment of language. Moreover, in patients presenting with memory loss, the amnesia may remain the prominent symptom for many years (amnestic AD), whereas in others, memory loss is combined at an early stage with other cognitive deficits (multidomain AD).[3] Mixed presentation of isocortical symptoms affecting multiple cognitive domains, including language, semantic, and attentional deficits, is a common pattern in early-onset AD. Also, a clinicopathological study of early-onset dementia, which encompassed distinct presentations, elicited a sensitivity for detection of Alzheimer pathology of 97% and specificity of 100%,[4] suggesting that the clinical diagnosis

[1]Division of Informatics, Imaging and Data Sciences, University of Manchester, Wolfson Molecular Imaging Centre, Manchester, UK
[2]Division of Neuroscience and Experimental Psychology, University of Manchester, Manchester, UK
[3]Salford Royal NHS Foundation Trust, Salford, UK
[4]Department of Nuclear Medicine and Lehrstuhl für Geriatrie, Universitätsklinikum Essen, Essen, Germany

Corresponding author:
Karl Herholz, University of Manchester, Wolfson Molecular Imaging Centre, 27 Palatine Road, Manchester, England M20 3LJ, UK.
Email: karl.herholz@manchester.ac.uk

is reliable. AD subtypes with primary isocortical symptoms are sometimes called atypical presentations and, in contrast to the common amnestic subtype, are less associated with the ApoE4 genotype.[5] These different genetic and phenotypic characteristics of AD subtypes raise the issue whether they actually share a common pathophysiology or represent different neurodegenerative diseases that only ultimately share the same deposits of pathological protein deposits.

Functional impairment in all AD subtypes can be explained by synaptic dysfunction, which is associated with impairment of regional glucose metabolism and can be investigated in-vivo by positron emission tomography (PET) using 18F-2-fluoro-2-deoxy-D-glucose (FDG). Regional impairment of glucose metabolism in the posterior cingulate cortex and temporo-parieto-occipital association areas has actually been described as the main finding in AD in many papers since 1980,[6] with predominant impairment of occipital visual association cortex in posterior cortical atrophy[7] and predominant impairment of temporoparietal language areas in logopenic aphasia.[8] Impairment of glucose metabolism in mesial temporal structures has been described less consistently, although hippocampal atrophy has been recognised as the most prominent finding in AD using MR morphometry. This has often tentatively been explained as a consequence of the limited spatial resolution of PET in combination with the small size and relative low normal metabolism of the hippocampus and associated structures.

Another important functional aspect of AD is the impairment of neuronal networks. These have been analysed primarily by EEG, functional MRI (fMRI) and diffusion tensor imaging (DTI).[9–12] These techniques investigate correlated brain signals primarily within individuals followed by pattern analysis across individuals. Network connectivity in AD has also been studied with FDG,[13–18] primarily analysing correlations of regional brain metabolic activity across subjects.[19,20] Thus, network structures and properties revealed by different methods are different,[21,22] even though EEG, fMRI and FDG PET commonly use signals associated with synaptic function and tend to share some large-scale topographical distributions.[23]

The aim of the present study was to investigate the differences and commonalities between AD with respect to focal metabolic impairment and associated networks using FDG PET as a firmly established functional imaging technique in AD. To overcome some limitations of previous FDG PET studies of AD subtypes,[7,8,24,25] we did not use a reference region or global cortical average for data normalisation. Instead we used a linear mixed effect models to account for differences in global and regional metabolism with subsequent analysis of residual correlations to study network alterations. Furthermore, we used a dedicated high-resolution brain scanner achieving a spatial resolution of 3 mm or better[26,27] for optimal representation of small but important structures, such as the hippocampus.

Methods

Study participants

Patients with a clinical diagnosis of Alzheimer's disease who met current diagnostic criteria[28] were included in the study. All patients had been assessed in a specialist neurological clinic for early onset dementia, and diagnosed with Alzheimer's disease based on clinical assessment, which includes a structured exploration of cognitive domains, neurological examination by a consultant neurologist and neuropsychological examination by a neuropsychologist specialising in dementia syndromes. Patients were excluded if they showed clinical characteristics of other neurodegenerative diseases that might mimic AD, such as dementia with Lewy bodies or corticobasal degeneration.

Patients fell into three clinically defined subtypes as described in detail by Kobylecki et al.[29] Amnestic patients ($n = 8$) presented with typical symptoms of poor recent memory, repetition in conversation, and better memory for the remote than recent past. Visual patients ($n = 8$) had dominant presenting symptoms of a visual, perceptual or spatial nature. Multidomain patients ($n = 9$) presented with problems in memory, with additional difficulties, particularly in language as early presenting characteristics consistent with the diagnostic category "language presentation" as described by McKhann et al.[28] Related neuropsychological assessment measures have been described previously.[29]

Nine healthy age-matched controls were drawn from an existing previously published neuroimaging dataset and used for comparison of FDG-PET data.[30] Demographic information of patients and controls is shown in Table 1.

Exclusion criteria included the presence of other significant neurological disease, history of significant head trauma with persistent neurological deficits or structural brain abnormalities, significant concomitant psychiatric disease, alcohol and substance abuse, and significant systemic illness or unstable medical condition. A Hachinski score of ≥ 4 was a contraindication to participation in the study.

All patients consented to participate in the study in accordance with the Guideline for Good Clinical Practice (GCP) issued by the National Institute for Health Research, UK. If their cognitive difficulties compromised literacy or their ability to assimilate and retain the purpose of the study, then informed written advice was sought from a personal consultee

Table 1. Subject characteristics.

	Amnestic AD (n = 8)	Multidomain AD (n = 9)	Visual AD (n = 8)	Controls (n = 9)	Test statistic (df), p value
Age (years)	62.9 ± 8.2	65.3 ± 7.1	59.8 ± 5.0	68.3 ± 5.5	F = 2.63 (3), $p = 0.069$
Duration (years)	5.2 ± 3.1	3.4 ± 1.9	2.9 ± 1.4	N/A	F = 2.12 (2), $p = 0.13$
Sex (F:M)	4:4	4:5	5:3	8:1	$p = 0.220$ [a]
Early onset AD	6/8	6/9	8/8	N/A	$p = 0.249$ [a]
APOE ε4 carriers	8/8	2/9	1/7	N/A	$P = 0.001$ [a]
MMSE	20.3 ± 3.5	16.8 ± 4.5	16.6 ± 4.6	29.7 ± 0.5	F = 25.17 (3), $p < 0.001$*
CDR (median, range)	0.75 (0.5-1.0)	0.5 (0.5-2.0)	1.0 (0.5-3.0)	N/A	F = 4.46 (2), $p = 0.108$
Cholinesterase inhibitor therapy	7/8	6/9	6/8	N/A	$P = 0.301$

[a]Fisher's exact test. *between controls and patients in post-hoc testing.

(usually the next of kin) under the provisions of the Mental Capacity Act 2005. The study was approved by South Manchester Research Ethics Committee (reference number: 09/H1003/77).

Imaging procedures

All patients underwent one MRI scan and one [18F]-FDG PET scan, the latter performed within two to four weeks of clinical assessment and MRI.

MRI

All MR imaging was performed on a 3.0 T Philips Achieva scanner (Philips Medical Systems, Best, Netherlands) using an eight-element sensitivity encoding spin echo (SENSE) head coil. T1-weighted 3D acquisition fast field echo (FFE) images were acquired with a 256×256 matrix, SENSE acceleration factor = 2, slice thickness 1 mm, 150 contiguous slices, reconstructed voxel size $1 \times 1 \times 1$ mm, TR = 8.4 ms, TE = 3.8 ms, TI = 1150 ms.

FDG-PET

[18F]-FDG PET imaging was performed on the high-resolution research tomograph (HRRT; CTI/Siemens) at Wolfson Molecular Imaging Centre, University of Manchester. Participants fasted for a minimum of 6 h prior to PET imaging. Participants were comfortably positioned within the scanner with gentle restriction of head movement by tape. A 7-min transmission scan prior to tracer injection and emission scan. Scanning was carried out in standardised quiet conditions, with low light, eyes closed and ears unplugged. A slow bolus intravenous injection of 370 MBq [18F]-FDG (10 ml) was given over 20 s 7 min subsequent to the start of the emission scan, followed by a slow bolus saline flush. PET data were acquired for a total of 60 min post-injection in list mode. Reconstruction of the acquired data was performed with an implementation of ordinary Poisson ordered subsets expectation maximization (OP-OSEM) available on the HRRT user community software.[31] Data were reconstructed with resolution modelling,[32] 12 iterations and 16 subsets resulting in images of matrix size $256 \times 256 \times 207$ and voxel size $1.22 \times 1.22 \times 1.22\,mm^3$. If head movement had been detected, correction by reframing and realignment of frames was applied.[33] Static summed images from 20 to 60 min post-injection were used for further analysis.

Region of interest PET analysis

Summed static PET images, smoothed at 2 mm full width at half maximum (FWHM) were co-registered to the T1-weighted MR scans in SPM8 (Statistical Parametric Mapping, Wellcome Trust Centre for Neuroimaging). Region-of-interest (ROI) analysis of major supratentorial grey matter areas was performed first by unified segmentation of structural T1-weighted MR images in SPM8, using a probabilistic anatomical atlas[34] which was spatially normalized to each individual subject's anatomical space (see Table 2 for a list of regions included). A grey matter object map was created by multiplying the normalized anatomical atlas with a grey matter binary mask, thresholded in native space at 0.5 (VINCI). Regional FDG activity values were extracted in ANALYZE 10.0 (Mayo Clinic Software).

According to the concept of standardised uptake values (SUV), regional FDG uptake values are

Table 2. List of ROIs included in the analysis, in the order of their loadings in the first principal component of normal controls.

1	Middle frontal gyrus
2	Inferolateral parietal cortex
3	Caudate nucleus
4	Thalamus
5	Posterior cingulate cortex (PCC)
6	Nucleus accumbens
7	Superior temporal gyrus, central part
8	Insula
9	Hippocampus
10	Anterior cingulate cortex
11	Superior temporal gyrus, anterior part
12	Amygdala
13	Putamen
14	Anterior temporal lobe, medial part
15	Posterior temporal lobe
16	Middle and inferior temporal gyri
17	Lateral occipital cortex
18	Anterior temporal lobe, inferolateral part
19	Parahippocampal and ambient gyri
20	Fusiform gyrus
21	Anterior orbital gyrus
22	Lateral orbital gyrus
23	Superior parietal gyrus
24	Orbitofrontal straight gyrus
25	Medial orbital gyrus
26	Posterior orbital gyrus
27	Postcentral gyrus
28	Precentral gyrus
29	Superior frontal gyrus
30	Cuneus
31	Lingual gyrus
32	Inferior frontal gyrus

expected to be proportional to injected dose and inversely related to body weight.[35] Due to the competition of tracer and unlabelled plasma glucose for the glucose transporter at the blood–brain barrier, there is also an inverse relation with plasma glucose.[36,37] We therefore converted regional FDG activity to SUV values for each subject with adjustment for plasma glucose levels, according to the following equation

$$SUV = \frac{Regional\ FDG\ activity}{Injected\ dose/Body\ weight} \times \frac{Plasma\ glucose}{Average\ plasma\ glucose} \quad (1)$$

Statistical methods

A linear mixed effect (LME) model[38] implemented in R (R Foundation, version 3.0.3, packages NLME and PHIA) was used first for the analysis the effects of injected dose, body weight and plasma glucose on regional tracer uptake, and second for the analysis of regional contrasts between groups.[39,40] Diagnostic groups, ROIs, and hemispheres (left/right) were defined as experimental variables, while global variation between individuals was absorbed by a random variable. Significance of experimental variables and their interactions was determined by marginal Wald F tests. Probability values for regional difference between groups were corrected for multiple comparisons.[41] Patterns of covariance of residual values between regions were analysed by principal component and correlation analysis (R modules "prcomp" and "corrplot").

Results

Demographic data

There were no significant differences in age or sex distribution between all groups. There also were no differences in disease duration, CDR, age of onset (early < 65 years vs late ≥ 65 years) or MMSE between patient groups (Table 1). MMSE was significantly lower in all patient groups compared to controls (all $p < 0.001$). The APOE $\varepsilon 4$ allele was present in all patients in the amnestic group and was significantly more frequent than in the other groups ($p = 0.001$). Comparable proportions of patients in each subtype group were taking cholinesterase inhibitors ($p > 0.05$).

Dependency of regional FDG uptake on systemic parameters

These multiplicative dependencies were tested for significance using an LME model relating the log-transformed regional values to the log-transformed values of dose, body weight and plasma glucose, with diagnostic groups, ROIs, and their interaction as fixed experimental variables, and individuals as random variable (Suppl. Table 1). Of the systemic parameters, only body weight (78.7 ± 13.0 kg) came out as significant ($p = 0.0013$), while injected dose and plasma glucose did not show a significant effect, probably due to the relatively narrow range of their values (360.0 ± 16.4 MBq, 5.15 ± 0.69 mmol/L, respectively). There were highly significant differences between ROIs ($p < 0.0001$) and their interaction with diagnostic groups ($p < 0.0001$), confirming the difference of regional patterns between diagnostic groups.

Regional metabolic impairment

The LME model for the analysis of regional SUVs included ROIs, hemispheres (L, R) and diagnostic groups as fixed experimental factors and individuals as a random factor. Also included were interactions between ROIs and groups, between ROIs and hemispheres, and between groups and hemispheres. The overall statistical results (Suppl. Table 2) again demonstrated a significant decrease of global metabolism that was similar in all patients groups ($p = 0.0447$, Figure 1). Groups showed highly significant differences of regional values and also of hemispheric asymmetries. Post hoc contrasts demonstrated that hemispheric asymmetries (with left hemispheric values lower than on the right) were significant in the multidomain and amnestic groups ($p < 0.0001$ and $p = 0.0002$, respectively), while there was no significant asymmetry in the visual group and in controls (Figure 1, Suppl. Table 3).

When checking individual regions, significant differences (with correction for multiple comparisons) were observed mainly between patients and controls (Suppl. Table 4). The only brain region with significant reduction in all patient groups was posterior cingulate gyrus (Figure 2(a)), and it was the only brain region showing significant hypometabolism in the amnestic subgroup. Hippocampus tended to show reduced metabolism in all subgroups but did not reach significance (Figure 2(b)). Multidomain and visual subgroups showed more extensive and severe regional hypometabolism than amnestic patients. This involved parietal, posterior temporal and lateral occipital regions (Suppl. Table 4, Figure 2(c) and (d)). As to be expected, the cuneus with the visual cortex was impaired in visual subgroup only.

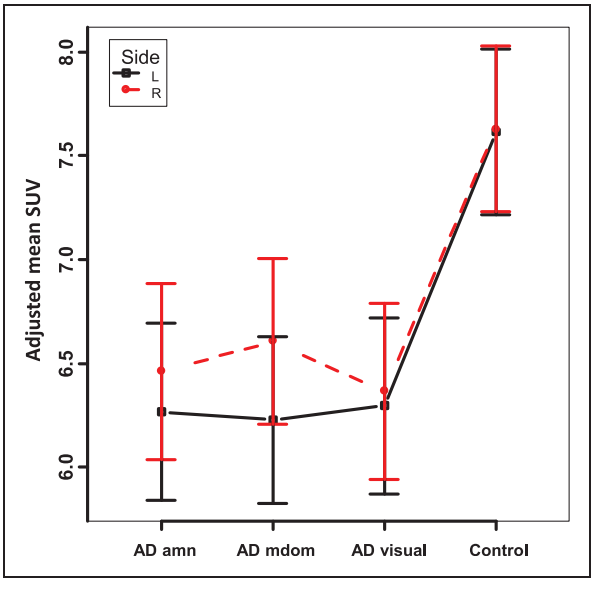

Figure 1. Mean SUV (average of all brain regions, with adjustment for plasma glucose; error bars indicating S.E.M.) by hemisphere and subject group.
amn: amnestic; mdom: multidomain.

Residual regional correlation patterns

A high proportion (61% and 64%, in left and right hemisphere, respectively) of regional covariance in normal controls was explained by the first principal component (PC1). Amnestic and multidomain patient groups tended to show lower proportions of covariance assigned to PC1 (amnestic 44% and 46%, multidomain 52% and 52%), while it was similar to controls in the visual AD group (61% and 63%).

As shown in Figure 3, high positive intercorrelations were seen within a large fronto-temporo-parietal cluster of regions comprising temporo-parieto-occipital association cortices, the middle frontal gyrus, some limbic structures, caudate nucleus and thalamus. It was negatively correlated with another cluster of regions comprising sensorimotor cortices, occipital (cuneus) and superior parietal and frontal regions involved in somatomotor and attention networks as well as orbitofrontal regions. Correlation patterns were very similar in the two hemispheres, and there was generally a high correlation between homologous regions in the hemispheres in controls (average $r = 0.84$), with some reduction in patients (amnestic 0.66, multidomain 0.71, visual 0.58).

Correlation patterns were different in patients compared to controls and each other, and region clusters tended to be smaller (Figure 4). However, a few correlations were well preserved. In particular, positive correlations between the middle frontal gyrus (region #1 in Table 2) and parietal association cortices (#2) including the posterior cingulate cortex (#5) persisted in all patient groups now also including superior parietal cortex (#23), which in controls had not been positively correlated. This group comprised mainly those regions that are metabolically impaired in patients. However, the normal strong positive correlation between posterior cingulate cortex (#5) and hippocampus (#9) was lost in all subtypes.

The most pronounced breakdown of the normal correlation pattern was observed in amnestic patients. For instance, the anterior cingulate cortex (#10), anterior temporal cortices (#11, 14, 18) became largely uncoupled from the network, and correlations of many regions with hippocampus (#9) and posterior cingulate cortex (#5) were reduced. Also, orbitofrontal areas (#21, 22, 24, 25, and 26) lost most positive correlations with other regions.

The correlation pattern in multidomain AD patients showed some preservation of correlations between

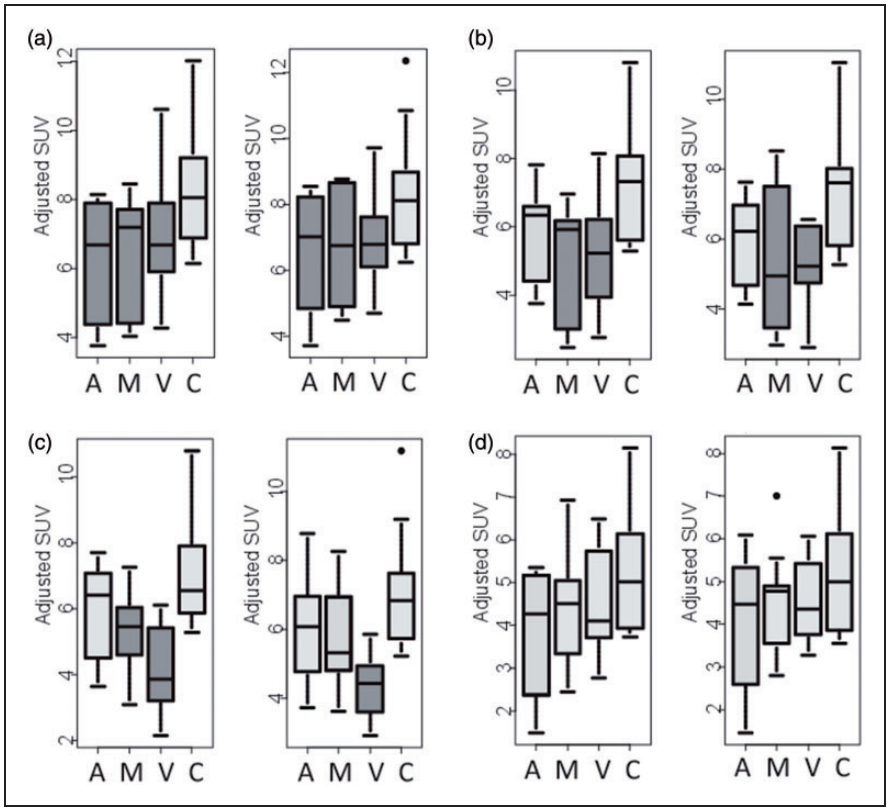

Figure 2. Box plots of FDG uptake (adjusted SUV) in selected brain regions (a: PCC, b: parietal cortex, c: lateral occipital cortex, d: hippocampus; left and right hemispheres, respectively). Groups are A: amnestic, M: multimodal, V: visual, and C: controls. Dark box fillings indicate a significant difference ($p < 0.05$) compared to controls.

temporal regions (#11, 14, 15, 16). Also, correlations were relatively well preserved in the somatomotor, attention and orbitofrontal cluster (#21 to 32) with the notable exception of the parietal lobe (#23).

In the visual subtype, the fronto-temporo-parietal cluster broke up into separate region groups, one comprising a fronto-parietal network (#1 and 2) with posterior cingulate (#5), thalamus (#4) and the striatum (#3 and 13), the other some of the rest (# 5 to 12 and 14 to 20) including most limbic and some default mode network regions. There was some preservation of correlations within the somatomotor network (#27 to 29), and between some orbitofrontal regions (#21 and 22) and the superior parietal lobe (#23).

Discussion

Most previous studies of regional metabolic activity using FDG PET in AD involved intensity normalisation of data by division through the values obtained in reference regions or by global averages. These approaches generally require the assumption that the reference regions are not affected by disease, which is often unknown or has even been disproved. For instance, the cerebellum is affected by crossed cerebellar diaschisis, which has been observed in AD, and global metabolism is reduced as the severity of AD and the extent of brain hypometabolism increase.[42] In contrast, the present analysis using an LME model[38,40] does not require such assumptions and actually demonstrated a significant reduction of standardized FDG brain uptake in patients. Glucose-adjusted SUV, as used in the present study, would be proportional to cerebral metabolic rates of glucose (CMRglc) under the assumptions that the lumped constant is constant and the injected dose divided by body weight is proportional to the cumulative arterial input function.[43] Partial volume effects due to regional brain atrophy may also contribute to apparent metabolic reduction. The lumped constant may vary in tumors and cerebrovascular disease,[44] and normalisation by body weight may fail dependent on age and in patient groups with systemic disorders that would change renal FDG excretion or deposition in other body organs (e.g. Hustinx et al.[45]). However, as our patient and control groups were homogeneous with regard to age and did not suffer from systemic disorders, the reduction in adjusted SUV probably reflects a reduction of global brain CMRglc to a similar degree as observed previously.[46]

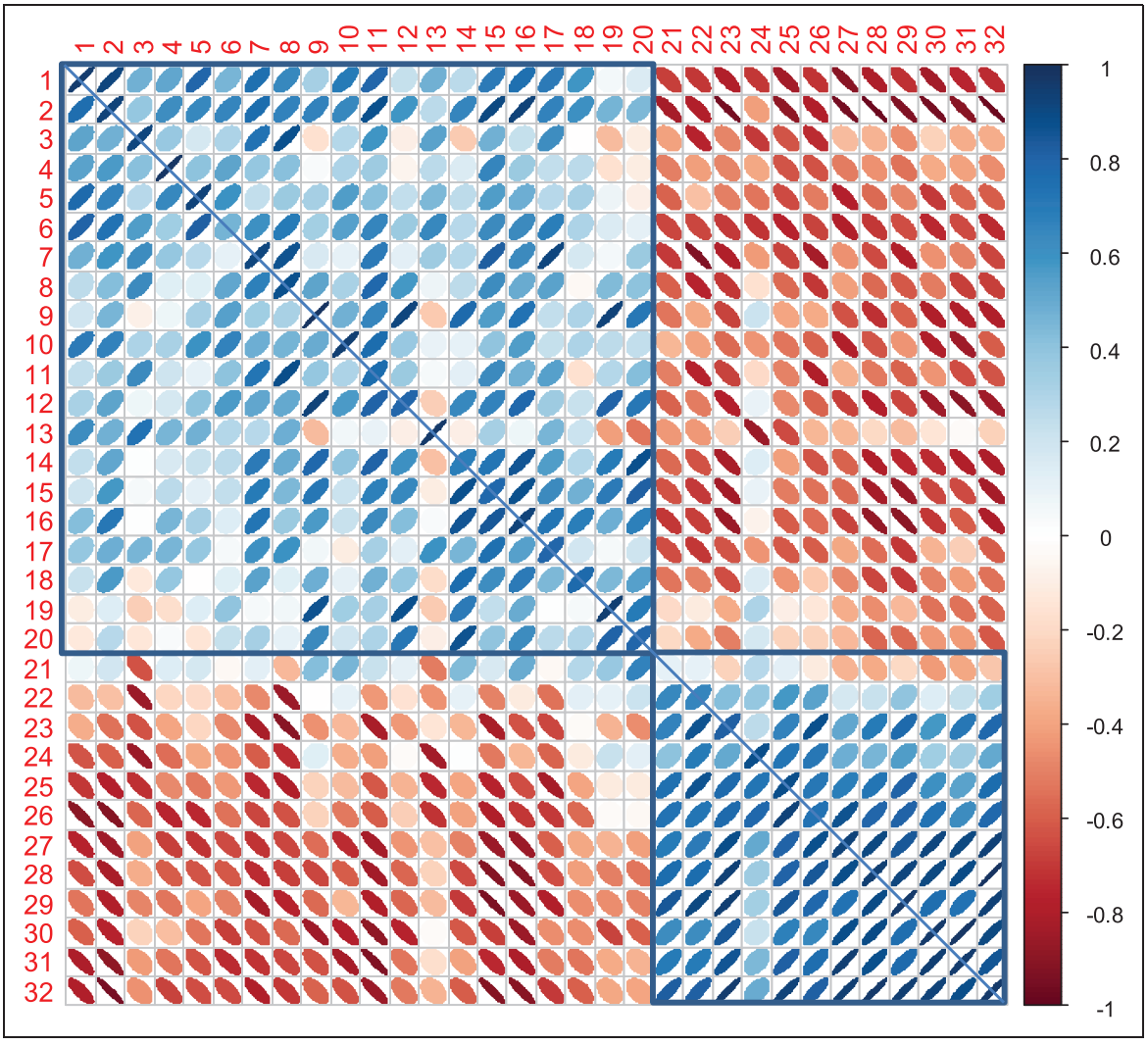

Figure 3. Ellipse plots of the metabolic regional correlation matrix in controls (see Table 2 for ROI order and numbers). Correlations within the left hemisphere are represented in the lower left part, interhemispheric correlations of homologous regions on the diagonal, and correlations within the right hemisphere in upper right part. Positive correlations are shown in blue, negative correlations in red. The two main clusters observed in controls are marked by blue boxes.

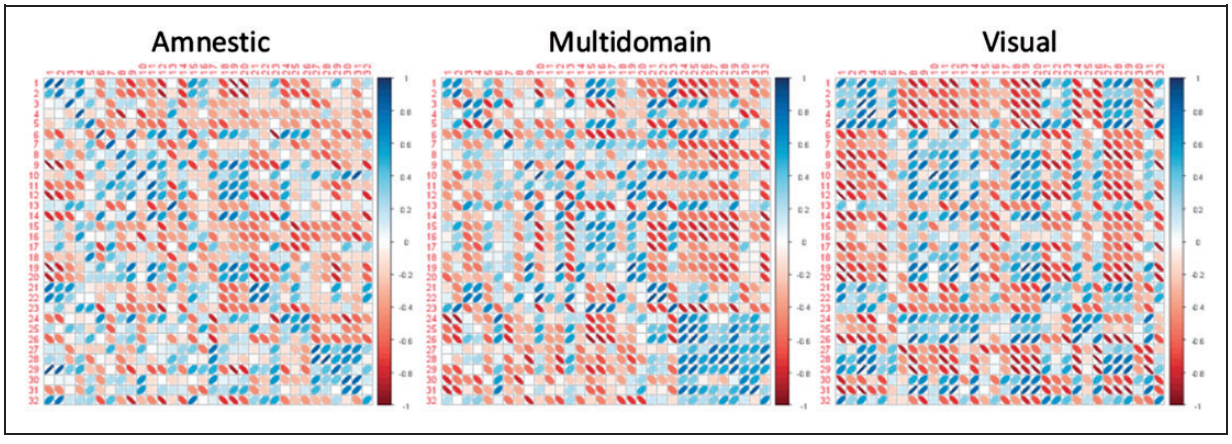

Figure 4. Ellipse plot of correlation matrices in patients, same arrangement as in Figure 3.

With respect to regional metabolic impairment, the present results reproduce some main findings previously reported in AD subtypes. For instance, these include prominent metabolic impairment of occipital cortex in the visual subtype, largely corresponding to findings described in posterior cortical atrophy.[7] Metabolic impairment of PCC, first highlighted by Minoshima et al.[47] stands out in the present study as a constant and similar finding across all subtypes. Thus, the present findings support the view that the PCC region, which has a high density of mitochondria, may be of particular pathophysiological relevance for AD.[48] Involvement of other association cortices appears to be facultative, at least at an early stage of the disease, depending on the particular subtype.

There is also confirmation of left hemispheric predominance of metabolic impairment, which has been noted in previous studies,[49] but it differs significantly between patient groups and is not present in the visual subtype. Thus, it does not appear to be an essential feature of AD and may again be more closely related to symptoms, which are clinically more evident when affecting the dominant hemisphere and therefore may cause a patient identification and selection effect at mild stages of AD.

On metabolic networks, our study confirms previous findings that, by identifying correlation patterns across individuals, they differ from structural, resting state fMRI, and electrophysiological networks,[22] and it would be beyond the scope of the present paper to discuss these in any detail. In our study, which is based on a relatively small number of subjects, essentially just two large clusters of positive correlations were identified in normal controls.

The largest cluster comprising fronto-temporoparietal association cortices also included PCC and hippocampus, similar to the findings of Morbelli et al.[13] A close correlation between PCC and hippocampus, two key structures of Papez's circuit, had also been identified in a principal component analysis of brain metabolic networks by Salmon et al.[50] In the present study, the correlation between these two structures was absent in all patient groups, supporting the view that impairment of their functional connection is a critical feature of AD.[30,51] Loss of this correlation is also remarkable as metabolic impairment in the hippocampus was generally relatively mild. In contrast, the metabolic correlation between frontal and temporoparietal association cortices was preserved in patient groups, similar to the findings of Klupp et al.[17]

Impairment of the metabolic networks in AD has been observed repeatedly since the pioneering study by Morbelli et al.[13] and Horwitz et al.[52,53] Numerically, less joint regional covariance is reflected in reduced variance covered by PC1.[54] This was also observed in our study within both hemispheres, and there was also a reduction of the interhemispheric correlations between homologous regions.

To our knowledge, this is the first study to look specifically at metabolic network differences between AD subtypes. Interestingly, the most pronounced network disruption was observed in amnestic patients even though they showed least impairment of specific cortical regions. This probably reflects the profound disruption of cognitive processes that is caused by memory impairment and the widely distributed extension of brain networks underpinning memory function.

Corresponding to the more focal cortical symptoms and associated regional metabolic impairment in multimodal and visual subtypes, they also showed preservation of some smaller metabolic correlation clusters. This preservation could be due to preservation of network function. For instance, somatomotor cortex function is known to be well preserved in AD, and thus preserved correlation clusters associated with it may also represent intact function, which in the case of multimodal AD would include orbitofrontal cortex and some frontal regions linked to maintaining attention. Obviously, that interpretation requires further studies as the number of subjects in each subtype group was small in this study and therefore the robustness of individual correlations is not ensured, while more detailed and targeted neuropsychological testing would also be required. It is also likely that some "preserved" metabolic correlations, especially those involving temporoparietal regions, actually reflect their joint involvement in the disease process.[17]

Our study predominantly represented early-onset AD, which allowed an approximately balanced representation of the three subgroups, while in late-onset patients, the amnestic group is typically much larger, vascular comorbidity is frequent, and metabolic networks differ from early-onset AD.[16] Inclusion of age as a covariate slightly increased the significance of the group main effect but did not otherwise change results (see Suppl. Table 1). Data quality was checked by inspection and Breusch-Pagan test of residuals (Suppl. Table 5/Figure1). Further studies are required to apply LME models to larger samples including late-onset patients to study metabolic effects of ApoE genotype, relation to specific cognitive symptoms, and cerebral microvascular disease, and to compare the proposed method with alternative approaches for data normalisation described in the literature.

In conclusion, PCC hypometabolism and impaired functional correlation between PCC and hippocampus was a common feature of all subtypes. It therefore appears to play a central role in the functional AD pathophysiology irrespective of subtypes. The amnestic subtype was characterised by the most severe network

alterations, while regional metabolic deficits were relatively mild. In contrast, the visual subtype presented with the most distinct regional metabolic deficits.

Funding

The author(s) disclosed receipt of the following financial support for the research, authorship, and/or publication of this article: The study was supported by a grant from Alzheimer Research UK.

Declaration of conflicting interests

The author(s) declared no potential conflicts of interest with respect to the research, authorship, and/or publication of this article.

Authors' contributions

Karl Herholz: conception, design, data acquisition, analysis, and interpretation, article drafting, final approval.
Cathleen Haense: data acquisition, analysis, and interpretation, revision and final approval.
Alex Gerhard: data acquisition and interpretation, article revision, final approval.
Matthew Jones: data acquisition and interpretation, article revision, final approval.
Jose Anton Rodriguez: data acquisition, article revision, final approval.
Shailendra Segobin: data analysis, article revision, final approval.
Julie Snowden: conception, design, data acquisition and interpretation, article revision, final approval.
Jennifer Thompson: data acquisition and interpretation, article revision, final approval.
Christopher Kobylecki: data acquisition, analysis and interpretation, article revision, final approval.

Supplementary material

Supplementary material for this paper can be found at the journal website: http://journals.sagepub.com/home/jcb

References

1. Murray ME, Graff-Radford NR, Ross OA, et al. Neuropathologically defined subtypes of Alzheimer's disease with distinct clinical characteristics: a retrospective study. *Lancet Neurol* 2011; 10: 785–796.
2. Galton CJ, Patterson K, Xuereb JH, et al. Atypical and typical presentations of Alzheimer's disease: a clinical, neuropsychological, neuroimaging and pathological study of 13 cases. *Brain* 2000; 123(Pt 3): 484–498.
3. Stopford CL, Snowden JS, Thompson JC, et al. Variability in cognitive presentation of Alzheimer's disease. *Cortex* 2008; 44: 185–195.
4. Snowden JS, Thompson JC, Stopford CL, et al. The clinical diagnosis of early-onset dementias: diagnostic accuracy and clinicopathological relationships. *Brain* 2011; 134(Pt 9): 2478–2492.
5. Snowden JS, Stopford CL, Julien CL, et al. Cognitive phenotypes in Alzheimer's disease and genetic risk. *Cortex* 2007; 43: 835–845.
6. Bohnen NI, Djang DS, Herholz K, et al. Effectiveness and safety of 18F-FDG PET in the evaluation of dementia: a review of the recent literature. *J Nucl Med* 2012; 53: 59–71.
7. Nestor PJ, Caine D, Fryer TD, et al. The topography of metabolic deficits in posterior cortical atrophy (the visual variant of Alzheimer's disease) with FDG-PET. *J Neurol Neurosurg Psychiatry* 2003; 74: 1521–1529.
8. Rabinovici GD, Jagust WJ, Furst AJ, et al. Abeta amyloid and glucose metabolism in three variants of primary progressive aphasia. *Ann Neurol* 2008; 64: 388–401.
9. Rombouts SA, Barkhof F, Goekoop R, et al. Altered resting state networks in mild cognitive impairment and mild Alzheimer's disease: an fMRI study. *Hum Brain Mapp* 2005; 26: 231–239.
10. Pandya S, Kuceyeski A and Raj A. The brain's structural connectome mediates the relationship between regional neuroimaging biomarkers in Alzheimer's disease. *J Alzheimers Dis* 2017; 55: 1639–1657.
11. Tam A, Orban P, Dansereau C, et al. Connectome-wide analysis of differences between normal aging, mild cognitive impairment, and dementia of the alzheimer's type using resting-state fmri connectivity. *Alzheimers Dement* 2014; 10: P827–P828.
12. Teipel S, Grothe MJ, Zhou J, et al. Measuring cortical connectivity in Alzheimer's disease as a brain neural network pathology: toward clinical applications. *J Int Neuropsychol Soc* 2016; 22: 138–163.
13. Morbelli S, Drzezga A, Perneczky R, et al. Resting metabolic connectivity in prodromal Alzheimer's disease. A European Alzheimer Disease Consortium (EADC) project. *Neurobiol Aging* 2012; 33: 2533–2550.
14. Toussaint PJ, Perlbarg V, Bellec P, et al. Resting state FDG-PET functional connectivity as an early biomarker of Alzheimer's disease using conjoint univariate and independent component analyses. *Neuroimage* 2012; 63: 936–946.
15. Carbonell F, Charil A, Zijdenbos AP, et al. Alzheimer's Disease Neuroimaging I. Hierarchical multivariate covariance analysis of metabolic connectivity. *J Cereb Blood Flow Metab* 2014; 34: 1936–1943.
16. Chung J, Yoo K, Kim E, et al. Glucose metabolic brain networks in early-onset vs. late-onset Alzheimer's disease. *Front Aging Neurosci* 2016; 8: 159.
17. Klupp E, Forster S, Grimmer T, et al. In Alzheimer's disease, hypometabolism in low-amyloid brain regions may be a functional consequence of pathologies in connected brain regions. *Brain Connect* 2014; 4: 371–383.
18. Titov D, Diehl-Schmid J, Shi K, et al. Metabolic connectivity for differential diagnosis of dementing disorders. *J Cereb Blood Flow Metab* 2017; 37: 252–262.
19. Lee DS, Kang H, Kim H, et al. Metabolic connectivity by interregional correlation analysis using statistical parametric mapping (SPM) and FDG brain PET; methodological development and patterns of metabolic connectivity in adults. *Eur J Nucl Med Mol Imaging* 2008; 35: 1681–1691.

20. Horwitz B. The elusive concept of brain connectivity. *Neuroimage* 2003; 19: 466–470.
21. Riedl V, Bienkowska K, Strobel C, et al. Local activity determines functional connectivity in the resting human brain: a simultaneous FDG-PET/fMRI study. *J Neurosci* 2014; 34: 6260–6266.
22. Di X and Biswal BB. Metabolic brain covariant networks as revealed by FDG-PET with reference to resting-state fMRI networks. *Brain Connect* 2012; 2: 275–283.
23. Lord LD, Expert P, Huckins JF, et al. Cerebral energy metabolism and the brain's functional network architecture: an integrative review. *J Cereb Blood Flow Metab* 2013; 33: 1347–1354.
24. Schmidtke K, Hull M and Talazko J. Posterior cortical atrophy: variant of Alzheimer's disease? A case series with PET findings. *J Neurol* 2005; 252: 27–35.
25. Madhavan A, Whitwell JL, Weigand SD, et al. FDG PET and MRI in logopenic primary progressive aphasia versus dementia of the Alzheimer's type. *PloS one* 2013; 8: e62471.
26. Wienhard K, Schmand B, Casey ME, et al. The ECAT HRRT: performance and first clinical application of the new high resolution research tomograph. *IEEE Trans Nucl Sci* 2002; 49: 104–110.
27. Olesen OV, Sibomana M, Keller SH, et al. Spatial resolution of the HRRT PET scanner using 3D-OSEM PSF reconstruction. In: *Nuclear Science Symposium Conference (Orlando, FL, USA) Record (NSS/MIC)*, Piscataway, NJ, USA, 2009, pp. 3789–3790. IEEE.
28. McKhann GM, Knopman DS, Chertkow H, et al. The diagnosis of dementia due to Alzheimer's disease: recommendations from the National Institute on Aging-Alzheimer's Association workgroups on diagnostic guidelines for Alzheimer's disease. *Alzheimer's Dement* 2011; 7: 263–269.
29. Kobylecki C, Haense C, Harris JM, et al. Functional neuroanatomical associations of working memory in early-onset Alzheimer's disease. *Int J Geriatr Psychiatry* 2017. Epub ahead of print 16 March 2017. DOI:10.1002/gps.4703.
30. Carter SF, Embleton KV, Anton-Rodriguez JM, et al. Regional neuronal network failure and cognition in late-onset sporadic Alzheimer disease. *Am J Neuroradiol* 2014; 35(6 Suppl): S18–S30.
31. Hong IK, Chung ST, Kim HK, Kim YB, Son YD and Cho ZH. Ultra fast symmetry and SIMD-based projection-backprojection (SSP) algorithm for 3-D PET image reconstruction. *IEEE Trans Med Imaging* 2007; 26: 789–803.
32. Sureau FC, Reader AJ, Comtat C, et al. Impact of image-space resolution modeling for studies with the high-resolution research tomograph. *J Nucl Med* 2008; 49: 1000–1008.
33. Segobin S, Matthews J, Williams S, et al. Motion detection from raw list-mode HRRT data and improved frame-by frame realignment for motion correction. *J Nucl Med* 2009; 50(Suppl): 589.
34. Heckemann RA, Hajnal JV, Aljabar P, et al. Automatic anatomical brain MRI segmentation combining label propagation and decision fusion. *Neuroimage* 2006; 33: 115–126.
35. Young H, Baum R, Cremerius U, et al. Measurement of clinical and subclinical tumour response und [18F]-fluorodeoxygluose and positron emission tomograpgy: review and 1999 EORTC recommendations. *Eur J Cancer* 1999; 35: 1773–1782.
36. Huang SC, Phelps ME, Hoffman EJ, et al. Noninvasive determination of local cerebral metabolic rate of glucose in man. *Am J Physiol* 1980; 238: E69–E82.
37. Ishizu K, Nishizawa S, Yonekura Y, et al. Effects of hyperglycemia on FDG uptake in human brain and glioma. *J Nucl Med* 1994; 35: 1104–1109.
38. Brown H and Prescott R. *Applied mixed models in medicine*, 3rd ed. Chichester, UK: Wiley, 2015.
39. Pinheiro JC and Bates DM. *Mixed effect models in S and S-plus*. New York: Springer, 2000.
40. Belda-Lois J-M and De Rosario Martínez H. Design of experiments for bioengineers in clinical settings. In: Pons JL and Torricelli D (eds) *Emerging therapies in neurorehabilitation*. Vol. 4. Springer Berlin Heidelberg, 2014, pp.329–345.
41. Yekutieli D and Benjamini Y. Resampling-based false discovery rate controlling multiple test procedures for correlated test statistics. *J Stat Plan Inference* 1999; 82: 171–196.
42. Yakushev I, Hammers A, Fellgiebel A, et al. SPM-based count normalization provides excellent discrimination of mild Alzheimer's disease and amnestic mild cognitive impairment from healthy aging. *Neuroimage* 2009; 44: 43–50.
43. Huang SC. Anatomy of SUV. Standardized uptake value. *Nucl Med Biol* 2000; 27: 643–646.
44. Baron JC, Frackowiak RS, Herholz K, et al. Use of PET methods for measurement of cerebral energy metabolism and hemodynamics in cerebrovascular disease. *J Cereb Blood Flow Metab* 1989; 9: 723–742.
45. Hustinx R, Smith RJ, Benard F, et al. Can the standardized uptake value characterize primary brain tumors on FDG-PET? *EurJ Nucl Med* 1999; 26: 1501–1509.
46. Kumar A, Newberg A, Alavi A, et al. Regional cerebral glucose metabolism in late-life depression and Alzheimer disease: a preliminary positron emission tomography study. *Proc Natl Acad Sci USA* 1993; 90: 7019–7023.
47. Minoshima S, Giordani B, Berent S, et al. Metabolic reduction in the posterior cingulate cortex in very early Alzheimer's disease. *Ann.Neurol* 1997; 42: 85–94.
48. Valla J, Berndt JD and Gonzalez-Lima F. Energy hypometabolism in posterior cingulate cortex of Alzheimer's patients: superficial laminar cytochrome oxidase associated with disease duration. *J Neurosci* 2001; 21: 4923–4930.
49. Loewenstein DA, Barker WW, Chang JY, et al. Predominant left hemisphere metabolic dysfunction in dementia. *Arch Neurol* 1989; 46: 146–152.
50. Salmon E, Kerrouche N, Perani D, et al. On the multivariate nature of brain metabolic impairment in Alzheimer's disease. *Neurobiol Aging* 2009; 30: 186–197.
51. Villain N, Desgranges B, Viader F, et al. Relationships between hippocampal atrophy, white matter disruption,

and gray matter hypometabolism in Alzheimer's disease. *J Neurosci* 2008; 28: 6174–6181.
52. Horwitz B, Grady CL, Schlageter NL, et al. Intercorrelations of regional cerebral glucose metabolic rates in Alzheimer's disease. *Brain Res* 1987; 407: 294–306.
53. Sanabria-Diaz G, Martinez-Montes E and Melie-Garcia L. Glucose metabolism during resting state reveals abnormal brain networks organization in the Alzheimer's disease and mild cognitive impairment. *PloS One* 2013; 8: e68860.
54. Pagani M, Giuliani A, Oberg J, et al. Predicting the transition from normal aging to Alzheimer's disease: a statistical mechanistic evaluation of FDG-PET data. *Neuroimage* 2016; 141: 282–290.